Characterization of Poly(vinylidene Fluoride) Nanofiber-Based Electrolyte and Its Application to Dye-Sensitized Solar Cell with Natural Dyes

Nita Kusumawati[1*], Pirim Setiarso[1], Agus Budi Santoso[2], Supari Muslim[2], Qurrota A'yun[1], and Marinda Mayliansarisyah Putri[1]

[1]*Department of Chemistry, Faculty of Mathematics and Natural Sciences, Universitas Negeri Surabaya, Jl. Ketintang, Surabaya 60231, Indonesia*

[2]*Department of Electrical Engineering, Faculty of Engineering, Universitas Negeri Surabaya, Jl. Ketintang, Surabaya 60231, Indonesia*

* ***Corresponding author:***

email: nitakusumawati@unesa.ac.id

Received: June 12, 2022
Accepted: October 17, 2022

DOI: 10.22146/ijc.75357

Abstract: *The potential of dye-sensitized solar cells (DSSC) as an alternative to depleting fossil fuels has been investigated. To optimize performance and efficiency, the effectiveness of PVDF and PVDF nanofiber (NF) membrane-based electrolytes in suppressing solvent leakage and evaporation in liquid electrolyte systems was evaluated. SEM results for PVDF NF membranes showed the formation of a network with a three-dimensional structure with a diameter of 100–300 nm and an average thickness of 0.14 mm. The Infrared (IR) spectrum shows the electrolyte and polymer-PVDF interactions. Differential Scanning Calorimetry (DSC) curve shows the melting transition of PVDF NF 7.66% lower than PVDF. Efficiency and resistance of DSSC based on natural dyes as measured by multimeter and Electrochemical Impedance Spectroscopy (EIS) at a solar intensity of 100 mW/cm² showed the highest efficiency of anthocyanin-based DSSC from telang (*Clitoria ternatea *L.) flower extract. Its use as a photosensitizer in an electrolyte system based on PVDF NF membranes resulted in an efficiency that was not significantly different from that of liquid electrolytes (1.69%).*

Keywords: *DSSC; natural dye; electrolyte; PVDF; PVDF NF*

■ INTRODUCTION

Energy, especially electrical energy, is one of the main drivers of a country [1-2]. Despite being one of the main needs of the community, the availability of electrical energy still depends on petroleum, natural gas, and various sources of fossil fuels which are getting depleted [3]. As an alternative, the use of solar cell technology is very promising [4]. The sensitization capability of wide band gap semiconductors by photosensitizer enables solar cell technology to convert solar energy into electrical energy [5]. High energy conversion efficiency and low electricity production costs compared to silicon solar cells make DSSC attracts a lot of research interest [6]. DSSC consists of two conductive glasses with three important components: a wide band gap semiconductor porous film with a dye molecule as a photosensitizer, a platinum (Pt) counter electrode, and a redox electrolyte [7-9]. In the DSSC system, photo-excitation of the dye produces electrons which are then injected into the titanium dioxide (TiO_2) semiconductor conduction band, while the redox reaction occurring at the interface of electrons is transferred to the counter electrode by an external circuit will result in regeneration of the oxidized photosensitizer dye [1].

The dye is one of the determining factors for the performance of DSSC, where its efficiency is influenced by the absorption spectrum and the loss of dye on the TiO_2 surface. Excellent conversion efficiency, chemical stability, and intense charge transfer absorption across the ultraviolet-visible (UV-Vis) light spectrum make ruthenium polypyrrole complexes one of the most effective photosensitizers. However, the metal content, which is not only relatively expensive but also harmful

to the environment, is the main weakness of this photosensitizer. Natural organic dyes from various plant species, such as chlorophyll, have been widely developed as an inexpensive alternative to ruthenium [5]. Chlorophyll from spinach leaves and *Sambucus ebulus* was reported to produce an electrical efficiency value of 1.15% in the DSSC system [10]. The presence of many chromophores in their molecular structure makes anthocyanins, betaxanthin, and braziline potential natural photosensitizer candidates for further development. Therefore, in this study, standardization of the use of anthocyanins from *telang* flower extract, betaxanthin from turmeric extract, and braziline from sappan wood bark extract as a natural photosensitizer for DSSC.

On the other hand, an electrolyte is one of the determining factors for DSSC stability. In DSSCs with liquid electrolytes, stability limits their wide commercialization [11-12]. Although it provides higher efficiency than gel and solid electrolytes, problems such as leakage, evaporation of volatile solutions, and iodine sublimation make liquid electrolytes have short-term stability [13]. To improve the DSSC stability, several studies were carried out for the polymer electrolytes development. High ionic conductivity, solvent-free, and flexibility are the advantages of this electrolyte. With a network capable of producing an ionic conductivity nearly as high as that of a liquid electrolyte and a solid structure with high mechanical resistance, the utilization of this electrolyte has the potential to reduce evaporation and leakage, thus, providing physical stability to the DSSC [14].

Poly(vinylidene fluoride) (PVDF) is a polymer with high electrochemical resistance and mechanical strength compared to other polymers, such as poly(vinyl chloride), polyacrylonitrile, and poly(methyl methacrylate). Sahito et al. reported the use of PVDF membrane-based electrolytes that is promising in the future because even though they have a 1.9% decrease in efficiency compared to liquid electrolytes, they have much better stability [15]. However, its hydrophobic nature reduces the I^-/I_3^- ionic mobility in the PVDF. To increase mobility, the use of PVDF NF membrane made by the electrospinning method is an ideal choice [16]. Increasing the mobility of ions in the membrane can increase the stability and electrical efficiency of the DDSC circuit. The dominance of amorphous structures in PVDF NF membranes has the potential to produce higher ionic conductivity than in PVDF membranes. By combining the use of PVDF and PVDF NF membrane-based electrolytes as an effective electrolyte trap and the use of anthocyanins, betaxanthin, and braziline as natural photosensitizers, the DSSC system is not only expected to be able to minimize leakage and produce better performance and efficiency but also be more eco-friendly than the previous DSSC system.

■ EXPERIMENTAL SECTION

Materials

Several materials with specifications that were used in this study were ethylene carbonate (EC) anhydrous (99%) and propylene carbonate (PC) anhydrous (99.7%), both obtained from Sigma Aldrich (USA); Iodine (I_2) (≥ 99.8%), nitric acid (HNO_3) (≥ 99.9%), Poly(vinylidene fluoride) powder (Mw~534,000), acetone (≥ 99.5%) from Sigma Aldrich (Singapore); potassium iodide (KI) (≥ 99%) and *N*,*N*-Dimethylacetamide (DMAc) (≥ 99%) from Merck (Belgium); Titanium dioxide (TiO_2) nanopowder (21 nm; 99.5%) from Sigma Aldrich (China); polyethylene glycol (PEG-1000) (Mw 1000) from Merck (Germany); Tween-80 from PT. Brataco Chemika (Indonesia); and Fluorine-doped Tin Oxide (FTO) glass (resistivity 10 Ω) were obtained from Changchun Yutai Optics Co., Ltd. (China).

Instrumentation

The instruments included a rotary evaporator (Buchi R-300), magnetic stirrer (NESCO LAB MS-H280-Pro), UV-Vis spectrophotometer (Shimadzu UV-1800), Fourier Transform Infrared (FTIR) spectrophotometer (Perkin Elmer Spectrum Two), Scanning Electron Microscope (SEM) (Zeiss EVO MA-10), Differential Scanning Calorimetry (DSC) (Linseis STA PT-1000), Voltammetry (797 VA Computrace Metrohm), Multimeter (Krisbow KW08-267).

Procedure

Natural photosensitizer

Natural photosensitizer was prepared by the maceration method. Natural dye material is immersed in a solvent in a ratio of 1:6. The maceration results were evaporated using a Buchi R-300 rotary evaporator. The natural dye concentrate is then stored at a temperature of 20–25 °C and ready to be used as a natural photosensitizer for DSSC.

Electrolyte solution

A total of 9.2 mg I_2; 0.06 g KI; 0.4 g EC; and 0.4 g PC; were mixed and stirred using NESCO LAB MS-H280-Pro magnetic stirrer (100 rpm; 30 min) to prepare an electrolyte solution.

Electrolyte polymer

PVDF membranes are made by a phase separation method followed by a casting knife and electrospinning casting techniques. As much as 18% (w/v) of PVDF has dissolved in DMAc and acetone (3:2) mixture by stirring for 12 h (65 °C; 270 rpm). The solution was cast on a glass plate with a thickness of 0.4 mm at 30 °C for 5 min pre-immersion, then immersed in 1000 mL aquadest for 30 min. The solid PVDF membrane was washed and dried for 24 h. Specifically, the electrospinning casting method was run at a voltage of 15 kV, the injector and drum collector distance of 15 cm, and a flow rate of 1 mL/h for 5 h.

Making of TiO_2 paste

A mixture of 0.2 g TiO_2, 0.4 mL 0.1 M HNO_3, 0.08 g PEG-1000, and 0.05 mL Tween-80 were stirred at 100 rpm for 30 min to produce a TiO_2 paste.

Fabrication of DSSC

The DSSC consists of two glasses: an FTO anode and an FTO cathode. The FTO anode glass has an active surface area of 3 cm^2. The TiO_2 paste was coated on the glass by the doctor blade method, then sintered for 1 h at 450 °C. The TiO_2 photoanode was cooled and then immersed in 10 mL of natural dye for 24 h. PVDF and PVDF NF membranes immersed in 1 mL of electrolyte for 1 h were coated on a carbon-coated cathode FTO glass. Thus, the FTO/TiO_2/PVDF/Pt/FTO system is formed (see Fig. 1).

Characterization

The absorption spectrum of the natural UV photosensitizer was analyzed using Shimadzu UV-1800 UV-Vis Spectrophotometry. The infrared spectra of liquid electrolytes and PVDF and PVDF-NF membrane-based electrolytes were analyzed using Perkin Elmer Spectrum Two FTIR spectrometer with Attenuated Total Reflection (ATR) mode at 30 °C. Meanwhile, membrane morphology was analyzed by Zeiss EVO MA-10 Scanning Electron Microscopy. The electrolyte thermal stability was evaluated using Linseis STA PT-1000 Differential Scanning Calorimetry (DSC) at 70–170 °C with a 10 °C/min heating rate [1]. Band gap natural photosensitizers were analyzed based on the reduction and oxidation currents using 797 VA Computrace Metrohm Voltammetry. The sample solution was a mixture of 20 mL of a natural photosensitizer with 5 mL

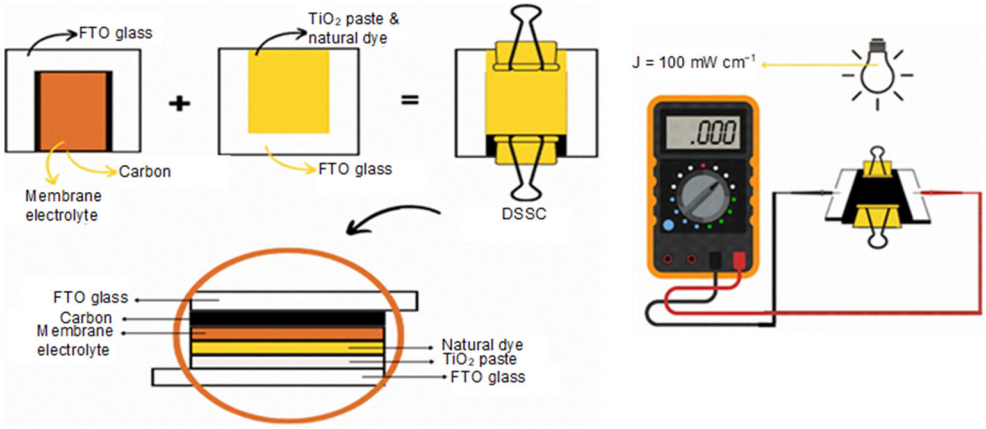

Fig 1. Schematic illustration of the DSSC fabrication

of potassium chloride (KCl) 0.3%. The efficiency of the DSSC circuit was analyzed based on the current and voltage obtained from measurements using a Krisbow KW08-267 Multimeter at 200 kΩ resistance and 200 mV voltage, while to get the effect of ionic conductivity on the J_{sc} value, an electron transport analysis was carried out, especially the interface resistance in the electrochemical system of the DSSC circuit using Gamry Reference 3000 Electrochemical Impedance Spectroscopy (EIS).

■ RESULTS AND DISCUSSION

Making Electrolyte Polymer

PVDF membranes are known for their good thermal and chemical stability. The low mass transfer resistance presented by its asymmetrical structure minimizes the fouling potential [17-19]. A phase inversion method is a promising option in this structure preparation due to its simple process and flexible production scale [20]. The selection of the right solvent is an absolute requirement to prevent particle aggregation in this preparation method. The minimum difference in solubility parameters indicates a high degree of compatibility with the solvent [21]. The solubility parameter values of PVDF, DMAc, and acetone are shown in Table 1.

The phase inversion step is induced using a non-solvent, namely water [22]. The high difference in the solubility parameters of PVDF-water (15.88 $MPa^{½}$), DMAc-water (25.23 $MPa^{½}$), and acetone-water (28.3 $MPa^{½}$) has caused PVDF-DMAc and PVDF-acetone systems thermodynamic equilibrium disturbances thus triggering phase separation. Diffusion of non-solvent in the casting solution produces a solid PVDF membrane [23].

Despite having various advantages, PVDF membranes are known to have crystallinity that has the potential to inhibit the movement of ions, resulting in low efficiency. Therefore, in this study, the effectiveness and efficiency of using electrolytes based on PVDF membranes with lower crystallinity will also be evaluated. PVDF NF has secondary structures such as a cavity and a core-shell [24]. PVDF NF can be made by various methods, one of which is electrospinning, which can produce hollow fibers and porous polymers [25]. The formation of NF is influenced by several factors, namely polymer concentration, preparation conditions (temperature, time, and stirring speed), solvent, and aging time [26-27]. With the method used, NF with perfect fibers has been obtained without beads and fiber defects. The addition of acetone can accelerate solvent evaporation and reduce the concentration of the casting solution to prevent further bead formation and conglutination [28].

Natural Dye Absorption

Anthocyanins, betaxanthins, carotenoids, chlorophyll, and flavonoids are some of the pigments that have a high potential to be used as natural photosensitizers in DSSC [29]. Natural dyes are one of the main components supporting the DSSC performance, known as low-cost solar cell technology [30]. Natural dyes are also known for their eco-friendly properties. When applied as a natural photosensitizer, each natural dye has a different sensitivity [31].

The classification of endemic plants spread and easily found throughout Indonesia makes turmeric (*Curcuma longa*) one of the sources of natural photosensitizer providers for DSSC. Turmeric is a natural dye containing betaxanthin pigment, which produces a yellowish orange [32]. To optimize the betaxanthin extraction, the suitability degree of 3 solvents with different polarities was investigated, namely

Table 1. Hansen solubility parameter

No	Material	δ_d ($MPa^{½}$)	δ_p ($MPa^{½}$)	δ_h ($MPa^{½}$)	δ_t ($MPa^{½}$)
1	PVDF	16	14.3	23.9	32.12
2	DMAc	16.8	11.5	10.2	22.77
3	Acetone	13.0	9.8	11.0	19.7
4	Water	12.2	22.8	40.4	48.0

distilled water, methanol, and ethanol. The maceration results show a yellow appearance in distilled water and orange in methanol as well as in ethanol [33].

Turmeric extract with distilled water showed absorbance at 502.3 nm (0.523), while 484.3 nm (0.744) and 462.3 nm (0.735) were indicated by methanol and ethanol, respectively. A higher absorbance value at 484.3 nm indicates a higher level of pigment solubility in methanol than in distilled water and ethanol. These findings are in line with publications reporting the maximum absorption of turmeric at 480 nm [34].

Braziline is a pigment that produces a red color [35]. With the abundant presence of this bark, braziline is also very potential to be used as a natural photosensitizer in DSSC. In this study, the water extract of sappan wood showed a red color, while the methanol and ethanol extract both showed a brick red color. The UV-Vis absorption spectrum of the sappan wood bark extract showed absorption peaks at 532.0 nm (0.223) for distilled water, 449.3 nm (0.506) for methanol, and 447.3 nm (0.539) for ethanol. In contrast to turmeric, the highest absorbance of the sappan bark extract was shown by ethanol. The dominant non-polar functional group in the sappan bark resulted in a higher degree of solubility of the braziline pigment in ethanol.

Telang flower is known to have high anthocyanin content. Anthocyanins are natural colorants from the flavonoid group, which give red, purple, and blue colors to vegetables, fruits, and wheat grains, almost tasteless and odorless [36-37]. Maceration of *telang* flower with aquadest produces a purple color, while maceration with methanol and ethanol both produce a bluish-green color. This bluish-green color is predicted to appear due to the combination of anthocyanin and chlorophyll pigments. However, the higher intensity of the green color indicates the dominant chlorophyll pigment in the methanol and ethanol extracts. Identification of the UV absorption of the *telang* flower extract showed an absorbance value of 0.176 at 574.3 nm; 0.164 at 621.9 nm; and 0.146 at 663.2 nm. The highest UV absorption at a wavelength of 574.3 nm indicates the good solubility of anthocyanins from *telang* flowers in distilled water. The polar nature of anthocyanins causes good solubility in aquadest, which has the highest level of polarity compared to methanol and ethanol [38].

Specifically, the spectrum of the *telang* flower dye extract in methanol showed the appearance of 2 absorbance peaks at 663.2 and 621.9 nm. This result is corroborated by the publication of Jeyaram and Geethakhrishna, who reported the maximum absorption of anthocyanins at 629 nm. This spectral region belongs to the anthocyanin resonance wavelength range, 520–700 nm. The more π-conjugated the anthocyanin structure, the stronger the color and the higher the absorption wavelength [39].

Hardeli et al. reported that anthocyanins are dyes that have a lot of π-conjugated. The more conjugate bonds, the more electrons are excited when exposed to light. Thus, the natural photosensitizer from the *telang* flower extract has the potential to produce high-efficiency DSSCs [40]. Furthermore, Ndeze et al. reported the ability of the carbonyl and hydroxyl groups of anthocyanins to retain color on the surface of TiO_2 and facilitate HOMO to LUMO electron transfer of dyes which were then transferred to the TiO_2 conduction band [41].

Band-Gap Energy of Natural Dye

Natural dyes must have a narrower band gap energy than the semiconductor energy (TiO_2; 3.2 eV for anatase and 3.0 eV for rutile phase) to be a photosensitizer so that the efficiency of the resulting DSSC is high. In the DSSC, there is a charge separation process [42]. Thus, it is important to determine the band gap energy value of the dye. The determination of the dye band gap energy follows the equation:

$$E_{HOMO} = -\left(E_{ox} + 4.4\right) \quad (1)$$

$$E_{LUMO} = -\left(E_{red} + 4.4\right) \quad (2)$$

$$\Delta E = LUMO - HOMO \quad (3)$$

The results are shown in Table 2.

The dye with the narrowest band gap energy has electrons with higher excitation potential. Thus, light sensitivity is also increased [43]. Anthocyanin pigments become dyes with many conjugate bonds. The more conjugated chains, the longer the electron resonance that occurs from the donor structure to the acceptor,

Table 2. Dyes band gap energy

Dye	Volta		
	HOMO	LUMO	Bandgap
Ethanol-sappanwood	-4.274	-2.934	1.379
Methanol-turmeric	-4.298	-2.907	1.395
Aquadest-turmeric	-4.299	-2.905	1.395
Aquadest-*telang* flower	-4.895	-3.713	1.182
Methanol-*telang* flower	-5.396	-3.357	2.038

resulting in a narrower band gap energy. Thus, making anthocyanin pigments have the highest potential for improving DSSC performance [44]. Table 5 shows the energy values for the widest band gap produced by the *telang* flower extract in methanol (2.038 eV) and the narrowest obtained by the *telang* flower extract in distilled water (1.182 eV).

Scanning Electron Microscopy (SEM)

Fig. 2 shows the PVDF and PVDF NF (d 100–300 nm) polymer electrolyte surface morphology. In the manufacture of PVDF NF polymer by electrospinning method, parameters such as voltage, tip distance from a collector, and polymer concentration are parameters that build surface morphology and fiber diameter on nanofiber membranes. Significant differences between PVDF and PVDF NF polymer electrolytes are shown in Fig. 2(a) and 2(b). Differences were observed in the formation of nanofiber fibers, larger pore size, higher porosity, and lower particle density of PVDF NF compared to PVDF. The SEM images also provide information on the formation of fine NF without beads at 18% by weight of the composition. This is in line with that published by Prasad et al. [45].

To obtain high mechanical strength and stability, the presence of cross-links in the nanofiber network is the most promising option because the increase in the density of the electrolyte-trapping polymer particles poses a significant obstacle to the electron flow rate in the DSSC system. Therefore, polymer electrolytes based on PVDF NF has better application potential in DSSC circuit systems than PVDF [1].

Photovoltaic Studies

As shown in Table 3, the performance of natural photosensitizer-based DSSC was determined by analysis

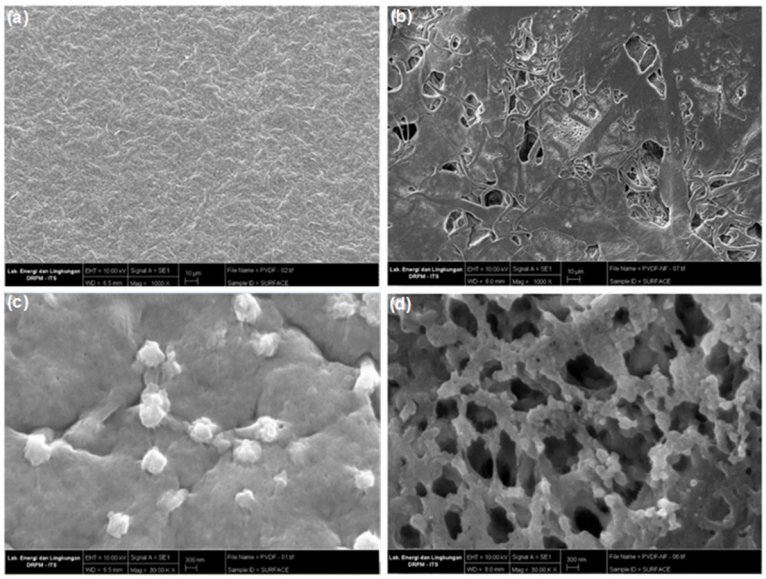

Fig 2. Electrolyte polymer surface morphology of the (a) PVDF 10,000×; (b) PVDF NF 10,000×; (c) PVDF 30,000×; (d) PVDF NF 30,000×

of open circuit voltage (V_{oc}), short circuit current density (J_{sc}), fill factor (FF), and efficiency (η) based on previously published equations [46]. Furthermore, the effect of using a combination of dyes and various electrolytes on the performance of natural photosensitizer-based DSSC can be seen from the photocurrent-voltage curve presented in Fig. 3.

The photovoltaic parameters showed a higher ionic conductivity of the liquid electrolyte than the electrolyte trapped in the polymer. The presence of a polymer electrolyte in the charge transport system causes a decrease in the Pt/electrolyte interface recombination reaction, thereby reducing the short-circuit current [47].

Among the five types of dye variations used, the order of efficiency is T-A > S-E > T-M > T_u-M > T_u-A. *Telang* flower produced the highest efficiency, with 1.69% for liquid electrolyte, 1.6% for PVDF NF polymer electrolyte, and 1.23% for PVDF polymer electrolyte. The overall efficiency value is much higher compared to the DSSC system based on a braziline photosensitizer and liquid electrolyte with the highest efficiency of 0.034% published by Zulenda et al., a chlorophyll photosensitizer from pandan leaf extract and liquid electrolyte with an efficiency of 0.1% published by Al Alwani et al., a chlorophyll photosensitizer from spinach leaf extract and liquid electrolyte with an efficiency of 0.398% published by Kabir et al. [2,5-6]. High efficiency is generally determined by the pigment content and band gap value. Specifically, anthocyanin pigments contain chromophore and auxochrome (–COOH; –OH),

Table 3. Photovoltaic parameters of DSSC

No	Dye	J_{sc} (10^{-3} mA cm^{-2})			V_{oc} (mV)			FF (10^{-2} %)			η (%)		
		L	NF	P	L	NF	P	L	NF	P	L	NF	P
1	T_u-A	3.5	2.3	1.4	344	340	321	40.5	27.6	23.5	1.21	0.79	0.45
2	T_u-M	3.3	3.2	2.2	401	393	354	46.9	36.6	29.5	1.32	1.28	0.77
3	T-A	3.6	3.4	2.9	475	463	424	25.3	23.8	21.3	1.69	1.6	1.23
4	T-M	3.3	3.1	2.8	416	389	383	42.5	38.2	32.8	1.36	1.21	1.06
5	S-E	3.6	3.2	2.8	434	416	363	19.4	17.1	13.4	1.56	1.35	1.03

Notes. T_u: turmeric; T: telang flower; S: sappanwood; A: aquadest; M: methanol; E: ethanol; L: liquid electrolyte; NF: PVDF NF electrolyte; P: PVDF electrolyte

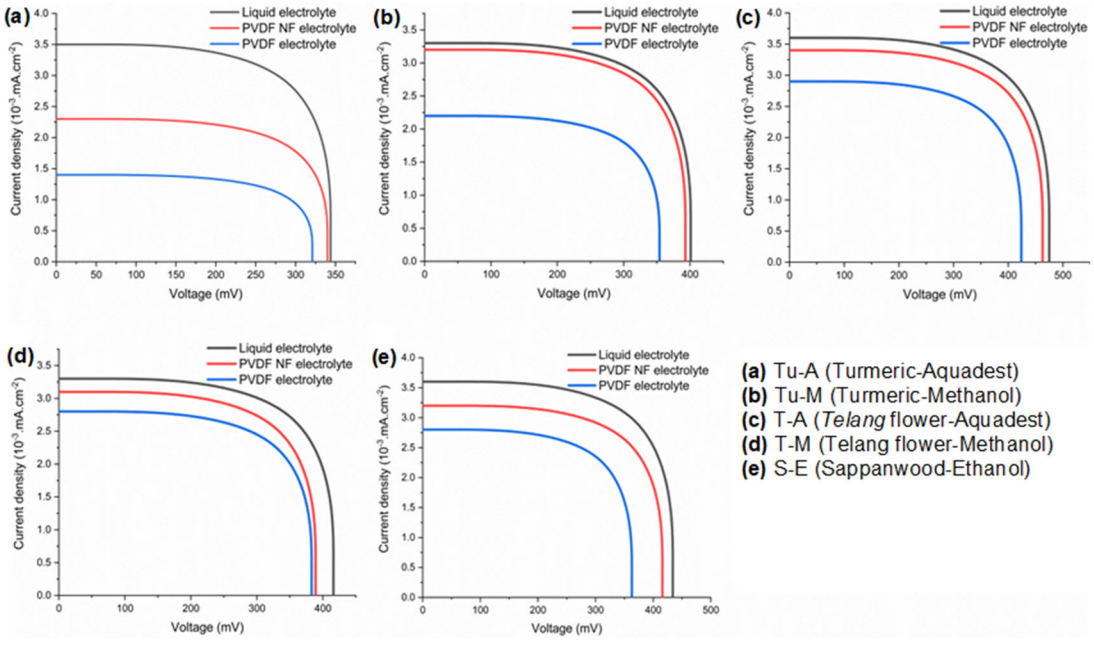

Fig 3. Photocurrent–voltage curve for DSSC sensitized by various extracts and electrolytes

which can absorb light in the energy range of UV visible light. Chromophores and auxochromes can attach to Ti(IV) sites on the TiO_2 surface, which supports electron transfer from anthocyanins to the TiO_2 conduction band [48]. In addition, the high number of conjugated chains in anthocyanins has triggered the electron resonance from the donor to acceptor to be longer, resulting in a narrow band gap value [1].

Electrochemical Impedance Spectroscopy

To get the effect of ionic conductivity on the J_{sc} value, an electron transport analysis was carried out by measuring the interface resistance in the electrochemical system of the DSSC circuit using EIS [49]. Injection of small amplitude in the form of voltage into the DSSC circuit is carried out to obtain voltage and current at a certain angle frequency in the form of a Nyquist plot [24-25].

EIS measurements resulted in the parameters R_s, R_{CT1}, and R_{CT2} of the FTO/TiO_2/dye/electrolyte/Pt/FTO configuration. R_S is the series resistance, R_{CT1} is the Pt/electrolyte interface charge transfer resistance, and R_{CT2} is the TiO_2/electrolyte interface charge transfer resistance [50].

$$Z_{DSSC} = R_S + \frac{R_{PT}}{1+(jw)^{nPT}R_{PT}CPE_{PT}} + \frac{R_{CT}}{1+(jw)^{nCT}R_{CT}CPE_{CT}} + R_D\sqrt{\frac{D_{Is}-J\delta^2}{j_\omega}}\tanh\sqrt{\frac{j_\omega}{D_{Is}-J\delta^2}} \quad (4)$$

where nPT is the constant phase element (CPE) referring to the counter electrode/electrolyte, nCT represents the photoanode/electrolyte interface, R_D is the Warburg diffusion resistance, and δ represents the effective diffusion length [51]. Table 4 shows the impedance measurement parameters of the DSSC circuit with electrolyte variations.

The impedance parameter values in Table 4 show the values of R_s, R_{CT1}, and R_{CT2} following the order of liquid electrolyte < PVDF NF-based electrolyte < PVDF based electrolytes. The high polymer content tends to create a 2D network, increasing the resistance for recombination reactions at the Pt/electrolyte and TiO_2/electrolyte interfaces. The polymer density of PVDF and PVDF NF can also effectively suppress the increased adhesion of the electrolyte to the counter electrode [52].

Charge transport kinetics in all three DSSC electrolytes can be used to predict the TiO_2 electron life by referring to Eq. (5).

$$\tau_r = \frac{1}{\omega_{max}} = \frac{1}{2\pi f_{max}}\tau_r \quad (5)$$

where ω_{max} is the angular frequency and f_{max} is the peak frequency. It was found that DSSC with a liquid electrolyte had a short electron life, whereas a PVDF and PVDF NF membrane electrolyte had a longer electron life. The results show that the excited electrons in liquid electrolyte-based cells recombine with I_3^- in electrolytes faster than in PVDF and PVDF NF membrane-based cells [53]. Thus, the photoelectron's lifetime (T) on the photoelectrode follows the order of the liquid < PVDF NF < PVDF membrane-based electrolyte. This result is in contrast to the electron recombination rate of the photoelectrode/electrolyte interface, which follows the order of liquid > PVDF NF > PVDF membrane-based electrolyte.

FTIR

To study the interactions of ions/polymers/solvents and electrolytes, chemical bonds and structures were analyzed using Fourier Transform Infrared (FTIR) Spectroscopy [54]. The PVDF and PVDF NF membrane IR spectra were compared in Fig. 4.

Table 4. Impedance parameters of DSSC

Electrolyte	R_s/Ω	R_{CT1}/Ω	R_{CT2}/Ω	T/ms	η/%
Liquid electrolyte	5.5	2.0	8.8	2.54	1.69
PVDF NF-based electrolyte	6.2	2.5	9.2	3.37	1.60
PVDF-based electrolyte	7.4	5.4	9.4	3.87	1.23

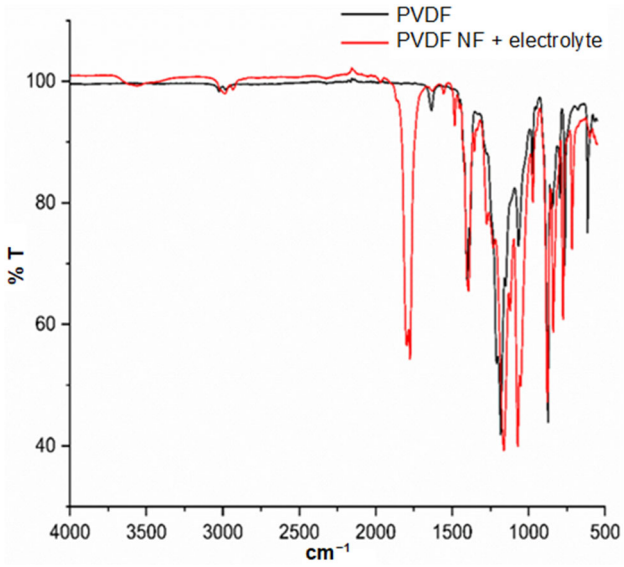

Fig 4. Infra-red spectra comparison of the PVDF and PVDF NF

PVDF is a semicrystalline thermoplastic polymer that has four crystalline phases, namely α, β, γ, and δ [55]. Bandara et al. publish the location of the α-phase and β-phase of pure PVDF [1]. Based on the publications of Saha et al., which report a typical peak of pure PVDF, the appearance of a peak of 841.15 cm^{-1} in the current work indicates CF_2 asymmetric stretching, while a peak at 873.09 cm^{-1} indicates the combined CF stretching, CF_2 stretching vibration, and CH_2 bending [56]. Peak appearance at 613.88 cm^{-1} indicates CF_2 bending and CCC skeletal vibrations in mixed mode. Respectively, the peak at 762.71 cm^{-1} indicates CH_2 rocking, while 795.97 cm^{-1} indicates CF_3 stretching vibration. The CF stretching at 975.61 and 1182.17 cm^{-1} also became the most significant peak marker for the PVDF crystal phase. Three peaks remain, namely at 1066.92; 1402.30; and 2984.09 cm^{-1}, showing CH bending, CH_2 wagging, and CH_2 asymmetric stretching, respectively. Several peaks indicating the amorphous phase of PVDF are also shown in Fig. 5.

By comparing the two, PVDF and PVDF NF, a slight shift in peak position was detected. For example, the appearance of a peak at 841.15 cm^{-1}, which is a marker of CF_2 asymmetric stretching in PVDF, shifted to 838.81 cm^{-1} in PVDF NF. Furthermore, a slight shift in the peak was also detected from 873.09 cm^{-1} to 875.84 cm^{-1}, which indicates a combination of CF stretching, CF_2 stretching vibration, and CH_2 bending in PVDF. The process of electrospinning on PVDF NF provides a lower level of crystalline as the cause of several shifts in peaks of the PVDF NF infra-red spectra.

Vibration bands of PVDF and PVDF NF amorphous phase were observed at certain wave numbers, although they did not seem clear. This condition is related to the interaction between the chains in the polymer. When mixed with the electrolyte, the polymers, in their interactions, are replaced by solvent-polymers. Because of that, the IR peaks associated with the amorphous phases of PVDF and PVDF NF appear insignificant for these electrolytes.

DSC Analysis

The large potential of DSSC utilization causes the analysis of the DSSC maximum operating temperature to be urgent to be carried out. Fig. 6 shows the DSC curves of EC, PC, PVDF membrane, PVDF, and PVDF NF membrane-based electrolyte at 60–170 °C. The results show the melting temperature of EC at 38.21 °C and PC above 170 °C. The low melting temperature of EC is one of the causes of high solvent evaporation in the electrolyte system, which triggers the low shelf life of the liquid electrolyte-based DSSC system [57-58].

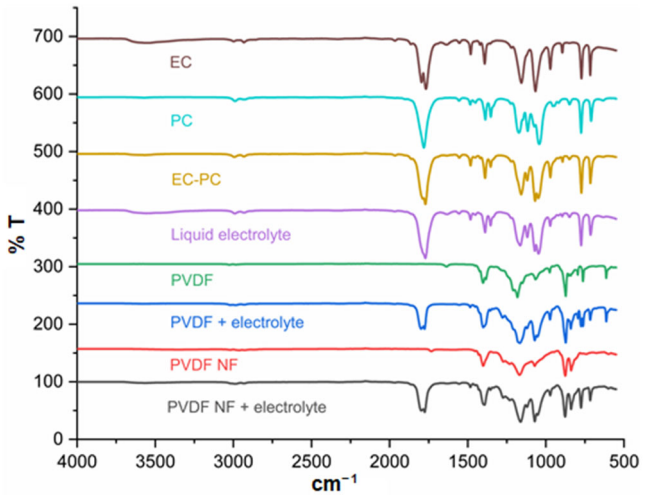

Fig 5. Infra-red spectra of PVDF and PVDF NF membrane, liquid electrolyte, PVDF and PVDF NF membrane-based electrolyte, EC-PC mixture, EC, PC (400–4000 cm^{-1})

Table 5. Melting enthalpy of PVDF and PVDF NF membrane electrolytes

Electrolyte	Peak area (mJ)	Weight (mg)	ΔH_m (Jg^{-1})	Relative crystallinity (%)
PVDF	57.18	23.04	2.48	2.31
PVDF NF	38.76	16.89	2.29	2.19

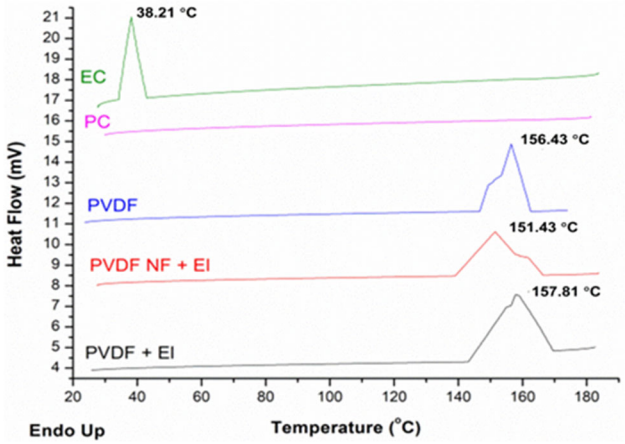

Fig 6. DSC thermograms (25–180 °C) of the EC, PC, PVDF membrane, PVDF, and PVDF NF membrane-based electrolyte

To determine the DSSC shelf life, the thermal stability of the PVDF and PVDF NF membrane-based electrolytes was investigated. The effectiveness of both types of membranes in producing a higher DSSC shelf life can be seen in the presence of liquid electrolytes in both membranes, even at temperatures above 100 °C. By comparing the DSC curve of the PVDF membrane with the PVDF and PVDF NF membranes-based electrolytes, it is found that the presence of liquid electrolytes in the membranes at temperature 157.81 °C on the PVDF membrane electrolyte system and 151.43 °C on the PVDF NF membrane electrolyte.

The broad endothermic peak at 130–160 °C indicates the melting of the polymer components in the electrolyte. This is in line with that published by previous researchers [59]. Specifically, the melting peak of PVDF was observed at a temperature of 157.81 °C, while that of PVDF NF was at 151.43 °C. The effect of nano-size was predicted as the cause of the lower melting temperature of PVDF NF compared to PVDF. In general, neither electrolyte shows a significant thermal transition up to 100 °C. Thus, the PVDF and PVDF NF electrolytes have thermal stability over the temperature range in which the solar cell operates.

Determination of relative crystallinity is done by calculating the melting enthalpy of PVDF and PVDF NF based on the peak area. The PVDF and PVDF NF melting enthalpies are 2.48 and 2.29 J g^{-1}, respectively. This value shows a 5.19% decrease in PVDF NF crystallinity compared to PVDF. PVDF with 100% crystallinity can be assumed to have a melting enthalpy of 107.4 J g^{-1}. Table 5 shows the relative crystallinity of each polymer electrolyte.

■ CONCLUSION

To make DSSC more environmentally friendly, in this work, the use of three natural pigment variants was evaluated, namely betaxanthin (484.3–502.3 nm), braziline (447.3 nm), and anthocyanin (574.3–621.9 nm). DSSCs with three types of electrolytes (liquid NF membrane-based electrolytes, PVDF, and PVDF NF) and natural photosensitizers were further characterized by measuring V_{OC}, J_{SC}, and FF, and EIS, the results were compared. The interaction of EC with cations in the three electrolytes showed the lowest prevalence of solvation (I^- by K^+) in the PVDF NF membrane-based electrolyte. This result is in line with the band shift of the polymer combination of 876 cm^{-1} in the FTIR spectra, which indicates a decrease in inter-chain interactions in the PVDF NF membrane-based electrolyte. The DSC thermogram showed that the melting peak of PVDF NF (151.43 °C) was lower than that of PVDF (157.81 °C). Nevertheless, in general, no significant thermal transitions were detected in the PVDF and PVDF NF electrolytes at the temperature at which the solar cells operate. Thus, the trapping of liquid electrolytes in the PVDF and PVDF NF membrane structures can be expected to suppress solvent leakage and evaporation, thereby potentially extending the shelf life of DSSC.

PVDF NF electrolyte-based DSSC and natural photosensitizer from *telang* flower extract offer the highest energy conversion efficiency (1.69%), with V_{OC} and J_{SC} values comparable to liquid electrolytes under the AM 1.5 solar irradiation standard. However, the impedance parameter values indicate that the high polymer content tends to create a 2D network, increasing the resistance for recombination reactions at the Pt/electrolyte and TiO_2/electrolyte interfaces. Decreasing the crystallinity of the PVDF NF membrane is expected to be a solution for this, while the simultaneous use of natural photosensitizers with varying absorption areas in the UV-Vis region is expected to increase light harvesting, which can further improve DSSC performance and efficiency.

■ ACKNOWLEDGMENTS

The author would like to thank the Indonesia Ministry of Education and Culture, Research and Technology of the Republic of Indonesia for providing financial support through national competitive research grants and the Department of Chemistry, Faculty of Mathematics and Natural Sciences Universitas Negeri Surabaya for providing research facilities support.

■ REFERENCES

[1] Bandara, T.M.W.J., Weerasinghe, A.M.J.S., Dissanayake, M.A.K.L., Senadeera, G.K.R., Furlani, M., Albinsson, I., and Mellander, B.E., 2018, Characterization of poly (vinylidene fluoride-*co*-hexafluoropropylene) (PVdF-HFP) nanofiber membrane based quasi solid electrolytes and their application in a dye sensitized solar cell, *Electrochim. Acta*, 266, 276–283.

[2] Zulenda, Z., Naselia, U.A., Gustian, N., Zaharah, T.A., and Rahmalia, W., 2018, Sintesis dan karakterisasi kompleks brazilin dari ekstrak kayu secang (*Caesalpinia sappan* Linn) serta aplikasinya dalam Dye Sensitized Solar Cells (DSSC), *J. Kim. Valensi*, 5 (1), 8–14.

[3] Roslan, N., Ya'acob, M., Radzi, M.A.M., Hashimoto, Y., Jamaludin, D., and Chen, G., 2018, Dye Sensitized Solar Cell (DSSC) greenhouse shading: New insights for solar radiation manipulation, *Renewable Sustainable Energy Rev.*, 92, 171–186.

[4] Sonker, R.K., Rahul, R., and Sabhajeet, S.R., 2018, ZnO nanoneedle structure-based dye-sensitized solar cell utilizing solid polymer electrolyte, *Mater. Lett.*, 223, 133–136.

[5] Al-Alwani, M.A.M., Mohammad, A.B., Kadhum, A.A.H., Ludin, N.A., Safie, N.E., Razali, M.Z., Ismail, M., and Sopian, K., 2017, Natural dye extracted from *Pandannus amaryllifolius* leaves as sensitizer in fabrication of dye-sensitized solar cells, *Int. J. Electrochem. Sci.*, 12, 747–761.

[6] Kabir, F., Sakib, S.N., and Matin, N., 2019, Stability study of natural green dye based DSSC, *Optik*, 181, 458–464.

[7] Kusumawati, N., Setiarso, P., and Muslim, S., 2018, Polysulfone/polyvinylidene fluoride composite membrane: Effect of coating dope composition on membrane characteristics and performance, *Rasayan J. Chem.*, 11 (3), 1034–1041.

[8] Önen, T., Karakuş, M.Ö., Coşkun, R., and Çetin, H., 2019, Reaching stability at DSSCs with new type gel electrolytes, *J. Photochem. Photobiol., A*, 385, 112082.

[9] Tan, C.Y., Farhana, N.K., Saidi, N.M., Ramesh, S., and Ramesh, K., 2018, Conductivity, dielectric studies and structural properties of P(VA-co-PE) and its application in dye-sensitized solar cell, *Org. Electron.*, 56, 116–124.

[10] Ahliha, A.H., Nurosyid, F., Supriyanto, A., and Kusumaningsih, T., 2018, Optical properties of anthocyanin dyes on TiO_2 as photosensitizers for application of dye-sensitized solar cell (DSSC), *IOP Conf. Ser.: Mater. Sci. Eng.*, 333, 012018.

[11] Pavithra, N., Velayutham, D., Sorrentino, A., and Anandan, S., 2017, Thiourea incorporated poly(ethylene oxide) as transparent gel polymer electrolyte for dye-sensitized solar cell applications, *J. Power Sources*, 353, 245–253.

[12] Dissanayake, M.A.K.L., Jaseetharan, T., Senadeera, G.K.R., Mellander, B.E., Albinsson, I., Furlani, M., and Kumari, J.M.K.W., 2021, Solid-state solar cells co-sensitized with PbS/CdS quantum dots and N719 dye and based on solid polymer electrolyte

with binary cations and nanofillers, *J. Photochem. Photobiol., A*, 405, 112915.

[13] Sundaramoorthy, K., Muthu, S.P., and Perumalsamy, R., 2018, Enhanced performance of 4,4'-bipyridine-doped PVDF/KI/I_2 based solid state polymer electrolyte for dye-sensitized solar cell applications, *J. Mater. Sci.: Mater. Electron.*, 29 (21), 18074–18081.

[14] Dissanayake, M.A.K.L., Divarathne, H.K.D.W.M.N.R., Thotawatthage, C.A., Dissanayake, C.B., Senadeera, G.K.R., and Bandara, B.M.R., 2014, Dye-sensitized solar cells based on electrospun polyacrylonitrile (PAN) nanofiber membrane gel electrolyte, *Electrochim. Acta*, 130, 76–81.

[15] Sahito, I.A., Sun, K.C., Arbab, A.A., and Jeong, S.H., Synergistic effect of thermal and chemical reduction of graphene oxide at the counter electrode on the performance of dye-sensitized solar cells, *Sol. Energy*, 190, 112–118.

[16] Sahito, I.A., Ahmed, F., Khatri, Z., Sun, K.C., and Jeong, S.H., 2017, Enhanced ionic mobility and increased efficiency of dye-sensitized solar cell by adding lithium chloride in poly(vinylidene fluoride) nanofiber as electrolyte medium, *J. Mater. Sci.*, 52 (24), 13920–13929.

[17] Ahmad, N.A., Goh, P.S., Yogarathinam, L.T., Zulhairun, A.K., and Ismail, A.F., 2020, Current advances in membrane technologies for produced water desalination, *Desalination*, 493, 114643.

[18] Kusumawati, N., Wijiastuti, A., and Santoso, A.B., 2015, Manufacture of PVDF-Kitosan composite membrane and its utilization in batik industrial wastewater treatment, *Res. J. Pharm., Biol. Chem. Sci.*, 6 (2), 495–503.

[19] Kusumawati, N., Setiarso, P., Sianita, M.M., and Muslim, S., 2018, Transport properties, mechanical behavior, thermal and chemical resistance of asymmetric flat sheet membrane prepared from PSf/PVDF blended membrane on gauze supporting layer, *Indones. J. Chem.*, 18 (2), 257–264.

[20] Maharani, K.D.A., and Kusumawati, N., 2016, The effect of casting solution and non-solvent composition on the performance of polysulfone membranes against chromium (VI), *Res. J. Pharm., Biol. Chem. Sci.*, 7 (2), 495–504.

[21] Ningrum, R.D.C., and Kusumawati, N., 2016, Development and characterization of polysulfone/polyvinylidene fluoride blend membrane induced by delayed liquid-liquid demixing, *Int. J. Adv. Sci. Eng. Inf. Technol.*, 6 (5), 716–722.

[22] Kusumawati, N., Setiarso, P., Muslim, S., and Purwidiani, N., 2018, Synergistic ability of PSf and PVDF to develop high-performance PSf/PVDF coated membrane for water treatment, *Rasayan J. Chem.*, 11 (1), 260–279.

[23] Guilen, G.R., Pan, Y., Li, M., and Hoek, E.M.V., 2011, Preparation and characterization of membranes formed by non-solvent induced phase separation: A review, *Ind. Eng. Chem. Res.*, 50 (7), 3798–3817.

[24] Mousavi, S.M., Zarei, M., Hashemi, S.A., Babapoor, A., and Amani, A.M., 2019, A conceptual review of rhodanine: Current applications of antiviral drugs, anticancer and antimicrobial activities, *Artif. Cells, Nanomed., Biotechnol.*, 47 (1), 1132–1148.

[25] Zhu, H., Wang, H., Wang, F., Guo, Y., Zhang, H., and Chen, J., 2013, Preparation and properties of PTFE hollow fiber membranes for desalination through vacuum membrane distillation, *J. Membr. Sci.*, 446, 145–153.

[26] Mousavi, S.M., Zarei, M., Hashemi, S.A., Ramakrishna, S., Chiang, W.H., Lai, C.W., Gholami, A., Omidifar, N., and Shokripour, M., 2020, Asymmetric membranes: A potential scaffold for wound healing applications, *Symmetry*, 12 (7), 1100.

[27] Ahmadi, S., 2020, Nanoparticles induced oxidative stress and related effects especially under exposure to electromagnetic radiations, *Adv. Appl. NanoBio-Technol.*, 1 (4), 91–98.

[28] Moshfeghian, M., Azimi, H., Mahkam, M., Kalaee, M.R., Mazinani, S., and Mosafer, H., 2021, Effect of solution properties on electrospinning of polymer nanofibers: A study on fabrication of PVDF nanofiber by electrospinning in DMAC and

(DMAC/Acetone) solvents, *Adv. Appl. NanoBio-Technol.*, 2 (2), 53–58.

[29] Ammar, M., Mohamed, H.S.H., Yousef, M.M.K., Abdel-Hafez, G.M., Hassanien, A.S., and Khalil, A.S.G., 2019, Dye-sensitized solar cells (DSSCs) based on extracted natural dyes, *J. Nanomater.*, 2019, 1867271.

[30] Enciso, P., Decoppet, J.D., Grätzel, M., Wörner, M., Cabrerizo, F.M., and Cerdá, M.F., 2017, A cockspur for the DSS cells: *Erythrina crista-galli* sensitizers, *Spectrochim. Acta, Part A*, 176, 91–98.

[31] Valaa, M., Krajčovič, J., Luňák, S., Ouzzane, I., Bouillon, J.P., and Weiter, M., 2014, HOMO and LUMO energy levels of *N*,*N*'-dinitrophenyl-substituted polar diketopyrrolopyrroles (DPPs), *Dyes Pigm.*, 106, 136–142.

[32] Sinha, D., De, D., and Ayaz, A., 2018, Performance and stability analysis of curcumin dye as a photosensitizer used in nanostructured ZnO based DSSC, *Spectrochim. Acta, Part A*, 193, 467–474.

[33] Choi, M., Noh, Y., Kim, K., and Song, O., 2016, Properties of dye sensitized solar cells with porous TiO_2 layers using polymethyl-methacrylate nano beads, *Korean J. Mater. Res.*, 26 (4), 194–199.

[34] Syafinar, R., Gomesh, N., Irwanto, M., Fareq, M., and Irwan, Y.M., 2015, Potential of purple cabbage, coffee, blueberry and turmeric as natural dyes for dye sensitive solar cells (DSSC), *Energy Procedia*, 79, 799–807.

[35] Nilesh, P.N., Rajput, M.S., Prasad, R.G.S.V., and Ahmad, M., 2015, Brazilin from *Caesalpinia sappan* heartwood and its pharmacological activities: A review, *Asian Pac. J. Trop. Med.*, 8 (6), 421–430.

[36] Martín, J., Navas, M.J., Jiménez-Moreno, A.M., and Asuero, A.G., 2017, "Anthocyanin Pigments: Importance, Sample Preparation and Extraction" in *Phenolic Compounds - Natural Sources, Importance and Applications*, Eds. Soto-Hernandez, Palma-Tenango, M., and Garcia-Mateos, R., IntechOpen, Rijeka, Croatia.

[37] Priska, M., Peni, N., Carvallo, L., and Ngapa, Y.D., 2018, Review: Antosianin dan pemanfaatannya, *Chakra Kimia*, 6 (2), 79–97.

[38] Hutagalung, R.A., Victor, V., Karjadidjaja, M., Prasasty, V.D., and Mulyono, N., 2014, Extraction and characterization of bioactive compounds from cultured and natural sponge, *Haliclona molitba* and *Stylotella aurantium* origin of Indonesia, *Int. J. Biosci., Biochem. Bioinf.*, 4 (1), 14–18.

[39] Jeyaram, S., and Geethakrishna, T., 2020, Vibrational spectroscopic, linear and nonlinear optical characteristics of *Anthocyanins* extracted from blueberry, *Results Opt.*, 1, 100010.

[40] Hardeli, H., Suwardani, S., Riky, R., Fernando, T., Maulidis, M., and Ridwan, S., 2013, Dye sensitized solar cells (DSSC) berbasis nanopori TiO_2 menggunakan antosianin dari berbagai sumber alami, *Proceedings of the Semirata FMIPA*, University of Lampung, 155–161.

[41] Ndeze, U.I., Aidan, J., Ezike, S.C., and Wansah, J.F., 2021, Comparative performances of nature-based dyes extracted from Baobab and Shea leaves photo-sensitizers for dye-sensitized solar cells (DSSCs), *Curr. Res. Green Sustainable Chem.*, 4, 100105.

[42] Dahlan, D., Leng, T.S., and Aziz, H., 2016, Dye-sensitized solar cells (DSSC) dengan sensitizer dye alami daun pandan, akar kunyit dan biji beras merah (black rice), *Jurnal Ilmu Fisika*, 8 (1), 1–8.

[43] Imelda, I., and Putri, R.A., 2020, Optimalisasi struktur π-konjugasi pada zat warna organic tipe D-π-A, *J. Res. Educ. Chem.*, 2 (2), 61–72.

[44] Maynez-Rojas, M.A., Casanova-González, E., and Ruvalcaba-Sil, J.L., 2017, Identification of natural red and purple dyes on textiles by Fiber-optics Reflectance Spectroscopy, *Spectrochim. Acta, Part A*, 178, 239–250.

[45] Prasad, G., Liang, J.W., Zhao, W., Yao, Y., Tao, T., Liang, B., and Lu, S.G., 2021, Enhancement of solvent uptake in porous PVDF nanofibers derived by a water-mediated electrospinning technique, *J. Materiomics*, 7 (2), 244–253.

[46] Sarker, S., Seo, H.W., and Kim, D.M., 2014, Calculating current density-voltage curves of dye-sensitized solar cells: A straight-forward approach, *J. Power Sources*, 248, 739-744.

[47] Kutlu, N., 2020, Investigation of electrical values of low-efficiency dye-sensitized solar cells (DSSCs), *Energy*, 199, 117222.

[48] Tractz, G.T., Viomar, A., Dias, B.V., de Lima, C.A., Banczek, E.P., da Cunha, M.T., Antunes, S.R.M., and Rodrigues, P.R.P., 2019, Recombination study of dye sensitized solar cells with natural extracts, *J. Braz. Chem. Soc.*, 30 (2), 371–378.

[49] Omar, A., Ali, M.S., and Abd Rahim, N., 2020, Electron transport properties analysis of titanium dioxide dye-sensitized solar cells (TiO_2-DSSCs) based natural dyes using electrochemical impedance spectroscopy concept: A review, *Sol. Energy*, 207, 1088–1121.

[50] Kim, K.H., Lee, S.M., Seo, M.H., Cho, S.E., Hwang, W.P., Park, S.H., Kim, Y.K., Lee, J.K., and Kim, M.R., 2012, Syntheses of organic dyes based on phenothiazine as photosensitizers and effects of their π-conjugated bridges on the photovoltaic performances of dye-sensitized solar cells, *Macromol. Res.*, 20 (2), 128–137.

[51] Bakri, A.S., Sahdan, M.Z., Adriyanto, F., Raship, N.A., Said, N.D.M., Abdullah, S.A., and Rahim, M.S., 2017, Effect of annealing temperature of titanium dioxide thin films on structural and electrical properties, *AIP Conf. Proc.*, 1778, 030030.

[52] Shah, S., Noor, I.M., Pitawala, J., Albinson, I., Bandara, T.M.W.J., Mellander, B.E., and Arof, A.K., 2017, Plasmonic effects of quantum size metal nanoparticles on dye-sensitized solar cell, *Opt. Mater. Express*, 7 (6), 2069–2083.

[53] Selvanathan, V., Yahya, R., Alharbi, H.F., Alharthi, N.H., Alharthi, Y.S., Ruslan, M.H., Amin, N., and Akhtaruzzaman, M., 2020, Organosoluble starch derivative as quasi-solid electrolytes in DSSC: Unravelling the synergy between electrolyte rheology and photovoltaic properties, *Sol. Energy*, 197, 144–153.

[54] Mokhtari, F., Latifi, M., and Shamshirsaz, M., 2015, Electrospinning/electrospray of polyvinylidene fluoride (PVDF): Piezoelectric nanofibers, *J. Text. Inst.*, 107 (8), 1037–1055.

[55] Osman, Z., and Arof, A.K., 2003, FTIR studies of chitosan acetate-based polymer electrolytes, *Elechtrochim. Acta*, 48 (8), 993–999.

[56] Saha, S., Yauvana, V., Chakraborty, S., and Sanyal, D., 2019 Synthesis and characterization of polyvinylidene-fluoride (PVDF) nanofiber for application as piezoelectric force sensor, *Mater. Today: Proc.*, 18, 1450–1458.

[57] Duh, Y.S., Lee, C.Y., Chen, Y.L., and Kao, C.S., 2016, Characterization on the exothermic behaviors of cathode materials reacted with ethylene carbonate in lithium-ion battery studied by differential scanning calorimeter (DSC), *Thermochim. Acta*, 642, 88–94.

[58] Hofmann, A., Wang, Z., Bautista, S.P., Weil, M., Müller, F., Löwe, R., Schneider, L., Mohsin, I.U., and Hanemann, T., 2022, Dataset of propylene carbonate based liquid electrolyte mixture for sodium-ion cells, *Data Brief*, 40, 107775.

[59] Shalu, S., Singh, V.K., and Singh, R.K., 2015, Development of ion conducting electrolyte membranes based on polymer PVdF-HFP, BMIMTFSI ionic liquid and the Li-salt with improved electrical, thermal and structural properties, *J. Matter. Chem. C*, 3 (28), 7305–7318.